Charmonium production in antiproton-nucleus reactions at low energies

A. B. Larionov,[1,2,*] M. Bleicher,[1,3] A. Gillitzer,[4] and M. Strikman[5]
[1]*Frankfurt Institute for Advanced Studies (FIAS), D-60438 Frankfurt am Main, Germany*
[2]*National Research Center "Kurchatov Institute," 123182 Moscow, Russia*
[3]*Institut für Theoretische Physik, J. W. Goethe-Universität, D-60438 Frankfurt am Main, Germany*
[4]*Institut für Kernphysik, Forschungszentrum Jülich, D-52425 Jülich, Germany*
[5]*Pennsylvania State University, University Park, Pennsylvania 16802, USA*
(Received 6 March 2013; revised manuscript received 16 April 2013; published 13 May 2013)

The $J/\Psi(1S)$ and $\Psi'(2S)$ production near threshold in antiproton-nucleus reactions is calculated on the basis of the Glauber model. The model takes into account the antiproton (pre-)absorption, proton Fermi motion, and charmonium formation length. We confirm an earlier prediction that the charmonium production in $\bar{p}A$ collisions at $p_{\rm lab} = 3$–$10\,{\rm GeV}/c$ is not influenced by formation length effects and is very well suited to determine the genuine charmonium-nucleon dissociation cross sections. The comparison is performed with the J/Ψ photoproduction at high energies, where formation length effects play a very important role. However, we demonstrate that the detailed structure of the proton and neutron density profiles has to be taken into account if one wants to extract information on the $J/\Psi N$ dissociation cross section from J/Ψ transparency ratios. These studies are relevant for the upcoming PANDA experiment at the Facility for Antiproton and Ion Research.

DOI: 10.1103/PhysRevC.87.054608 PACS number(s): 25.43.+t, 14.40.Lb, 24.10.Ht, 25.20.Lj

I. INTRODUCTION

The exploration of the properties of quantum chromodynamics (QCD) matter under extreme conditions is one of the most challenging endeavors of today's high-energy physics. The dynamics of heavy quarks, i.e., c and b quarks, and their bound states has been shown to provide new insights into these questions. A better understanding of the interactions of charmonia with cold nuclear matter is especially very important for the studies of charm production in heavy-ion collisions, in particular, of the J/Ψ suppression in a quark-gluon plasma [1]. The interpretation of J/Ψ yields from p-A and noncentral AA collisions at moderate energies ($\sqrt{s} =$ 17.3 GeV) in terms of a usual hadronic scenario requires the J/Ψ dissociation cross section on a nucleon to be about 6–7 mb [2,3]. Moreover, as stated in Ref. [2], such cross sections are consistent with the world data on J/Ψ transparency ratios from other reactions induced by elementary particles (γ, π, $\bar{p}$) on nuclei. However, if one takes into account contribution of J/Ψ produced in the decays of higher charmonium states and larger cross section of inelastic $\chi_c N$ interactions, the $J/\Psi N$ dissociation cross section turns out to be about 2 times smaller, i.e., about 3.5 mb [4].

A problematic feature of all existing experimental data on J/Ψ transparency ratios,

$$S_A = \frac{\sigma_{pA\to J/\Psi X}}{A\sigma_{pN\to J/\Psi X}}, \tag{1}$$

(here "p" denotes any kind of elementary projectile and N stands for the nucleon) in elementary particle-induced reactions is that the charmonia are produced at high momenta from about 20 GeV/c up to several TeV/c. Due to the large Lorentz boost of the charmonia, the existing data give access to only the interactions of prehadronic $c\bar{c}$ and $c\bar{c}g$ configurations with the nuclear medium which would transform into J/Ψ well after the target. Thus, the extracted value of the dissociation cross section needs to be studied in other kinematical situations, when the charmonium moves more slowly through the nuclear target.

Brodsky and Mueller [5] proposed to measure color transparency effects for J/Ψ production in $\bar{p}$-nucleus interactions, where the threshold beam momentum ($p_{\rm thr} = 4.07$ GeV/c for J/Ψ production in $\bar{p}p$ interactions) is quite low. The first theoretical study of this reaction has been done in Ref. [6] within the color diffusion and Glauber models taking into account the Fermi motion of the nucleons. The most important results of Ref. [6] are (i) the high sensitivity of the production cross section $\sigma_{\bar{p}A\to R(A-1)^*}$ of a charmonium state R, where R stands for J/Ψ, Ψ', or χ_c on a nucleus to the RN-dissociation cross section; (ii) due to the Fermi motion the cross section of charmonium production on a nucleus is strongly suppressed, i.e., $\sigma_{\bar{p}A\to R(A-1)^*} \sim (10^{-4}$–$10^{-3})Z\sigma_{\bar{p}p\to R}$ at the beam momentum of the on-shell R production;[1] and (iii) $\sigma_{\bar{p}A\to R(A-1)^*}$ is sensitive to the color transparency effect for the incoming antiproton (which can, however, be reformulated as a phenomenological treatment of $\bar{p}$ absorption) but insensitive to the color transparency for the produced J/Ψ and having modest sensitivity for heavier charmonium state R.

Later, in Ref. [7], the J/Ψ and Λ_c production in $\bar{p}A$ collisions at the Ψ' and J/Ψ production thresholds has been addressed with a focus on the effects of the nondiagonal transitions $\Psi' N \to J/\Psi N$. However, Fermi motion effects have been neglected in Ref. [7]. We also mention a very inspiring feasibility study at the Fermi National Accelerator Laboratory (Fermilab) [8], which presented the beam

*Corresponding author: larionov@fias.uni-frankfurt.de

[1]This estimate corresponds to the perfect beam resolution for $\bar{p}p$ collisions. See Eq. (20) below and the text after it.

momentum dependence of the charmonium production cross sections in $\bar{p}A$ collisions with heavy gas targets (CH_4, N, O, Ne, Ar, and Xe).

The main purpose of the present work is to perform a detailed theoretical analysis of the J/Ψ production in $\bar{p}A$ collisions near threshold. This is one of the subjects of the planned PANDA experiment at the Facility for Antiproton and Ion Research (FAIR) [9]. Comparisons of the J/Ψ transparency ratios in $\bar{p}A$ and γA reactions are performed with a focus on the sensitivity to the $J/\Psi N$ dissociation cross section.

Section II explains our model. The model predictions for the charmonium production in $\bar{p}A$ reactions are given in Sec. III with an emphasis on the sensitivity to the charmonium-nucleon dissociation cross sections. For comparison, we have also calculated the J/Ψ transparency ratios in photo-induced reactions and showed that the existing experimental data from Stanford Linear Accelerator Center (SLAC) for $E_\gamma = 20$ GeV [10] and, moreover, of Fermilab for $E_\gamma = 120$ GeV [11] do not allow us to constrain the $J/\Psi N$ dissociation cross section due to the formation length effects and large experimental errors. Finally, in order to evaluate the influence of multistep processes on J/Ψ production in $\bar{p}A$ reactions, the results obtained within the Giessen Boltzmann-Uehling-Uhlenbeck (GiBUU) model [12] are presented. The conclusions are given in Sec. IV.

II. MODEL

In the reaction $\bar{p}A \to R + X$ at beam momentum close to the charmonium R production threshold, the produced charmonium carries nearly the entire antiproton momentum. Therefore, we can apply a Glauber model similar to that of Ref. [6]. The cross section of the charmonium R production in a $\bar{p}A$ collision is given by

$$\sigma_{\bar{p}A\to R(A-1)^*} = 2\pi \int_0^\infty db\, b\, v_{\bar{p}}^{-1} \int_{-\infty}^{\infty} dz P_{\bar{p},\mathrm{surv}}(z,b) \times \Gamma_{\bar{p}\to R}(z,b) P_{R,\mathrm{surv}}(z,b), \quad (2)$$

where the integration is done over the antiproton impact parameter b and the longitudinal coordinate z. $v_{\bar{p}} = p_{\mathrm{lab}}/E_{\bar{p}}$ is the antiproton velocity with respect to the target nucleus. The in-medium width of the antiproton with respect to the charmonium production is

$$\Gamma_{\bar{p}\to R}(z,b) = \int \frac{2d^3p}{(2\pi)^3} v_{\bar{p}p} \sigma_{\bar{p}p\to RX}(p, p_{\bar{p}}) f_p(z,b,\mathbf{p}), \quad (3)$$

where $v_{\bar{p}p} = q\sqrt{s}/E_{\bar{p}}E_p$ is the antiproton-proton relative velocity with $q = \sqrt{s/4 - m^2}$ being the center-of-mass momentum of the antiproton and the proton at the center-of-mass energy of $\sqrt{s}$; $m = 0.938$ GeV is the nucleon mass. To simplify the discussion we use here the simplest model for the proton momentum distribution, i.e., the Fermi distribution $f_p(z,b,\mathbf{p}) = \Theta(p_{F,p} - |\mathbf{p}|)$, where $p_{F,p} = (3\pi^2\rho_p(z,b))^{1/3}$ is the local Fermi momentum of protons and ρ_p is the local proton density. The more realistic spectral function with correlations would slightly reduce the value of cross section near maximum and add momentum tails removing the sharp cutoffs. Currently the program of the experimental studies of the short-range correlations is under way at the TJNAF and models of the nuclear spectral functions incorporating these findings are being developed; for a recent review see Ref. [13]. This would allow in the near future to perform more accurate calculations of the rates of the charm production for the kinematics where $\bar{p}$ produces J/Ψ in the interaction with a fast nucleon.

If the beam momentum is close to that of exclusive R production at the mass pole, then all processes except $\bar{p}p \to R$ can be neglected, and one can use in Eq. (3) the exclusive resonance production cross section $\sigma_{\bar{p}p\to R}$ instead of the inclusive one, $\sigma_{\bar{p}p\to RX}$. For $\sigma_{\bar{p}p\to R}$ we apply the relativistic Breit-Wigner formula,

$$\sigma_{\bar{p}p\to R} = \frac{3\pi^2}{q^2}\sqrt{s}\Gamma_{R\to\bar{p}p}\mathcal{A}_R(s), \quad (4)$$

with the resonance spectral function

$$\mathcal{A}_R(s) = \frac{1}{\pi}\frac{\sqrt{s}\Gamma_R}{\left(s - m_R^2\right)^2 + s\Gamma_R^2}. \quad (5)$$

The remaining two important ingredients of Eq. (2) are the survival probability of the antiproton until it reaches the point (z,b),

$$P_{\bar{p},\mathrm{surv}}(z,b) = \exp\left[-\int_{-\infty}^{z} dz'\rho(z',b)\sigma_{\bar{p}N}^{\mathrm{inel}}(p_{\mathrm{lab}})\right], \quad (6)$$

and the survival probability of the charmonium R until it is emitted to the vacuum,

$$P_{R,\mathrm{surv}}(z,b) = \exp\left[-\int_{z}^{\infty} dz'\rho(z',b)\sigma_{RN}^{\mathrm{eff}}(p_R, z'-z)\right]. \quad (7)$$

In Eqs. (6) and (7), $\rho = \rho_p + \rho_n$ is the total nucleon density, $\sigma_{\bar{p}N}^{\mathrm{inel}}$ is the $\bar{p}N$ inelastic cross section

$$\sigma_{\bar{p}N}^{\mathrm{inel}}(p_{\mathrm{lab}}) = \sigma_{\bar{p}N}^{\mathrm{tot}} - \sigma_{\bar{p}N}^{\mathrm{el}}, \quad (8)$$

and $\sigma_{RN}^{\mathrm{eff}}$ is the charmonium-nucleon effective cross section, which will be explained below. The total and elastic antiproton-neutron cross sections in Eq. (8) are set equal to the antiproton-proton ones. The $\bar{p}p$ cross sections are taken from the PDG parametrization [14],

$$\sigma_{\bar{p}p}^{\mathrm{tot}}(p_{\mathrm{lab}}) = 38.4 + 77.6p_{\mathrm{lab}}^{-0.64} + 0.26\ln^2(p_{\mathrm{lab}}) - 1.2\ln(p_{\mathrm{lab}}), \quad (9)$$

$$\sigma_{\bar{p}p}^{\mathrm{el}}(p_{\mathrm{lab}}) = 10.2 + 52.7p_{\mathrm{lab}}^{-1.16} + 0.125\ln^2(p_{\mathrm{lab}}) - 1.28\ln(p_{\mathrm{lab}}), \quad (10)$$

where the beam momentum, p_{lab}, is in GeV/c and the cross sections are in mb.

Let us next turn to the time dependence of the charmonium formation. This is expressed via the charmonium-nucleon effective cross section, $\sigma_{RN}^{\mathrm{eff}}(p_R, z)$, which is a function of the charmonium momentum p_R in the target nucleus rest

frame and of the distance z from the $c\bar{c}$-pair production point. Following Refs. [6,15], we express $\sigma_{RN}^{\rm eff}$ in terms of a formation length l_R:

$$\sigma_{RN}^{\rm eff}(p_R,z) = \sigma_{RN}(p_R)\left(\left\{\left(\frac{z}{l_R}\right)^{\tau}+\frac{\langle n^2k_t^2\rangle}{m_R^2}\left[1-\left(\frac{z}{l_R}\right)^{\tau}\right]\right\}\times\Theta(l_R-z)+\Theta(z-l_R)\right) \quad (11)$$

with $\tau=1$. In Eq. (11), n is the number of hard gluons in the intermediate state and $\langle k_t^2\rangle^{1/2}\simeq 0.35$ GeV/c is the average transverse momentum of a quark in a hadron. Assuming that the reaction $\bar{p}p\to R$ is dominated by $qqq+\bar{q}\bar{q}\bar{q}$ annihilation into three hard gluons [5], we will use the value $n=3$. The formation lengths of hadrons are model dependent. For the J/Ψ we apply a standard formula with an energy denominator (cf. Refs. [4,6,15])

$$l_{J/\Psi}\simeq\frac{2p_{J/\Psi}}{m_{\Psi'}^2-m_{J/\Psi}^2}. \quad (12)$$

For Ψ' we rely on the estimate of Ref. [4],

$$l_{\Psi'}\simeq 6\ {\rm fm}\frac{p_{\Psi'}}{30\ {\rm GeV}}, \quad (13)$$

which, however, has large theoretical uncertainty.

Formula (3) for the partial width of the antiproton with respect to the process $\bar{p}p\to R$ can be simplified in the limit of small width of the resonance R. To this aim, we perform the integration over proton momentum in (3) using the spherical coordinate system with the z axis along the antiproton beam momentum,

$$\Gamma_{\bar{p}\to R}=\frac{3\Gamma_{R\to\bar{p}p}}{2}\int_0^{p_{F,p}}dpp^2\int_{-1}^{1}d\cos\Theta\,\frac{v_{\bar{p}p}}{q^2}\sqrt{s}\mathcal{A}_R(s), \quad (14)$$

where $\cos\Theta=p_z/p$ and $s=(E_p+E_{\bar{p}})^2-p^2-p_{\rm lab}^2-2pp_{\rm lab}\cos\Theta$. It is convenient to make the angular dependence in the spectral function explicit:

$$\mathcal{A}_R(s)=\frac{\gamma}{4\pi pp_{\rm lab}[(A(p)-\cos\Theta)^2+\gamma^2/4]}, \quad (15)$$

where $A(p)=[(E_p+E_{\bar{p}})^2-p^2-p_{\rm lab}^2-m_R^2]/2pp_{\rm lab}$ and $\gamma=\sqrt{s}\Gamma_R/pp_{\rm lab}$. If $\gamma\ll 1$, one can replace the Breit-Wigner distribution (15) by the δ-functional distribution,[2]

$$\mathcal{A}_R(s)\simeq\frac{1}{2pp_{\rm lab}}\delta[A(p)-\cos\Theta], \quad (16)$$

and set $\sqrt{s}\simeq m_R$ in Eq. (14). Substituting Eq. (16) in Eq. (14) and performing the integration over $\cos\Theta$ we obtain the following formula:

$$\Gamma_{\bar{p}\to R}=\frac{3m_R\Gamma_{R\to\bar{p}p}}{4p_{\rm lab}q_R^2}\int_{\min(p_1,p_{F,p})}^{\min(p_2,p_{F,p})}dp\,p\,v_{\bar{p}p}, \quad (17)$$

where $q_R=\sqrt{m_R^2/4-m^2}$. The limiting momenta, p_1 and p_2, are, respectively, the smaller and larger solutions of the equation $A(p)=\pm 1$.

In order to proceed further, we have to specify the dispersion relation between the energy and momentum of a proton in the target nucleus. The choice consistent with a model where nucleons carry all nucleus momentum in the infinite momentum frame is to set the proton energy constant independent on the proton momentum, i.e., $E_p=m-B$, where $B\simeq 8$ MeV is the nucleus binding energy per nucleon (in actual calculations we used the nucleus-dependent empirical values of the binding energies from Ref. [16]). In this case, using the expression $v_{\bar{p}p}=q_Rm_R/E_{\bar{p}}E_p$ allows us to take the momentum integral in Eq. (17) analytically,

$$\Gamma_{\bar{p}\to R}=\frac{3m_R^2\Gamma_{R\to\bar{p}p}}{8p_{\rm lab}E_{\bar{p}}E_pq_R}\left[\min(p_2,p_{F,p})^2-\min(p_1,p_{F,p})^2\right], \quad (18)$$

with $p_{1,2}=|p_{\rm lab}\mp\sqrt{(E_{\bar{p}}+E_p)^2-m_R^2}|$. Since $p_2\gg p_{F,p}$, we can replace the upper integration limit in Eqs. (17) and (18) by $p_{F,p}$. At the beam momentum of the on-shell R production on the proton in vacuum at rest, $p_1\simeq 0$ and Eq. (18) simplifies to

$$\Gamma_{\bar{p}\to R}^{\rm on-shell}\simeq\frac{3m_R^2\Gamma_{R\to\bar{p}p}p_{F,p}^2}{8p_{\rm lab}E_{\bar{p}}E_pq_R}. \quad (19)$$

Thus, $\Gamma_{\bar{p}\to R}^{\rm on-shell}\propto\rho_p^{2/3}$. The deviation from the usual linear density dependence originates from the narrowness of the resonance state R: Due to the Fermi motion it is difficult to find a proton which exactly matches the on-shell resonance kinematics.

Equation (19) leads to the estimate of Ref. [6] for the ratio

$$\frac{\sigma_{\bar{p}A\to R(A-1)^*}}{Z\sigma_{\bar{p}p\to R}}\simeq\frac{3\pi m_Rm\Gamma_R}{4(m_R^2-2m^2)v_{\bar{p}}p_{F,p}}\sim 10^{-4} \quad (20)$$

for $\Gamma_R\simeq 93$ keV in the case of J/Ψ. Such a strong reduction implies, however, the antiproton energy being precisely on the R on-shell peak, i.e., $E_{\bar{p}}=m_R^2/2m-m$ (or $p_{\rm lab}=m_Rq_R/m$). If the beam energy resolution ΔE does not allow us to resolve the on-shell R production in the $\bar{p}p\to R$ reaction, i.e., $\Delta E\gg\Gamma_R$, the right-hand side of Eq. (20) should be multiplied by $2m\Delta E/\pi m_R\Gamma_R$ (see also Ref. [6]). We emphasize that the beam energy resolution is strongly influencing the elementary cross section $\sigma_{\bar{p}p\to R}$, but not the cross section on the nucleus $\sigma_{\bar{p}A\to R(A-1)^*}$, since the latter changes on the rather large scale $\Delta E\sim p_{F,p}\sim 0.3$ GeV only.

III. RESULTS

We will consider the following target nuclei: ^{9}Be, ^{12}C, ^{16}O, ^{27}Al, ^{40}Ca, ^{56}Fe, ^{63}Cu, ^{75}As, ^{112,116,120,124}Sn, ^{142}Ce, ^{181}Ta, ^{197}Au, and ^{208}Pb. This choice is mostly motivated by the availability of neutron density parameters [17–19].

[2]Since $p\simeq p_{F,p}\simeq 0.3$ GeV/c, we obtain the estimate $\gamma\sim 10^{-4}$ for the J/Ψ and Ψ' charmonium states. We have also checked in some selected cases that the direct (however, extremely CPU-time-consuming) Monte Carlo calculation of the momentum integral in Eq. (3) gives results indistinguishable from those obtained assuming zero width of the charmonium states.

TABLE I. Neutron density parameters (in fm) for some of the nuclei used in calculations. For ^{9}Be and ^{181}Ta nuclei, the neutron matter density while for Sn isotopes the point neutron density parameters are given.

Nucleus	R_n	a_n
^{9}Be	2.11	1.000
^{181}Ta	6.42	0.640
^{112}Sn	5.416	0.543
^{116}Sn	5.399	0.552
^{120}Sn	5.356	0.565
^{124}Sn	5.530	0.558

For light nuclei ($A \leqslant 20$) we use the proton and neutron density profiles of the harmonic oscillator model

$$\rho_q(r) = \rho_q^0\left[1 + a_q\left(\frac{r}{R_q}\right)^2\right]\exp\{-(r/R_q)^2\}, \quad q = p, n. \tag{21}$$

For heavy nuclei ($A > 20$) we apply the two-parameter Fermi distributions

$$\rho_q(r) = \rho_q^0\left[\exp\left(\frac{r - R_q}{a_q}\right) + 1\right]^{-1}, \quad q = p, n. \tag{22}$$

The normalization constants ρ_q^0 are chosen such that

$$\int d^3r\rho_p(r) = Z, \quad \int d^3r\rho_n(r) = A - Z. \tag{23}$$

The charge-density-distribution parameters are taken from a standard compilation [20]. The neutron density parameters for most of nuclei are taken from Nieves *et al.* [18], who report the fits to the Hartree-Fock calculations with the density-matrix expansion [21]. In the present calculations we use the *point* density parameters of protons and neutrons which were obtained from charge density parameters and neutron matter density parameters by employing the correction formulas from Ref. [18].

The neutron density parameters for some of the nuclei used in our calculations are, however, not given in Ref. [18]. For ^{9}Be and ^{181}Ta we rely on the Glauber model analysis of 1-GeV proton charge-exchange scattering by Koptev *et al.* [17], while for Sn isotopes we employ the results of the antiprotonic x-ray analysis of Schmidt *et al.* [19]. The neutron density parameters of these nuclei are collected in Table I.

The main features of the antiproton-nucleus interaction with a heavy nucleus leading to the exclusive J/Ψ production are visualized in Fig. 1, which shows the $\bar{p}$ survival probability $P_{\bar{p},\mathrm{surv}}$, the partial J/Ψ production width $\Gamma_{\bar{p}\to J/\Psi}$, and their product as functions of z at the two different values of an impact parameter for the ^{181}Ta target. The beam momentum 4.07 GeV/c is chosen to set the produced J/Ψ on-shell for the proton target at rest. Thus, according to Eq. (19), $\Gamma_{\bar{p}\to J/\Psi} \propto \rho_p^{2/3}$. As expected, the antiproton is almost completely absorbed in the diffuse surface region, where the partial

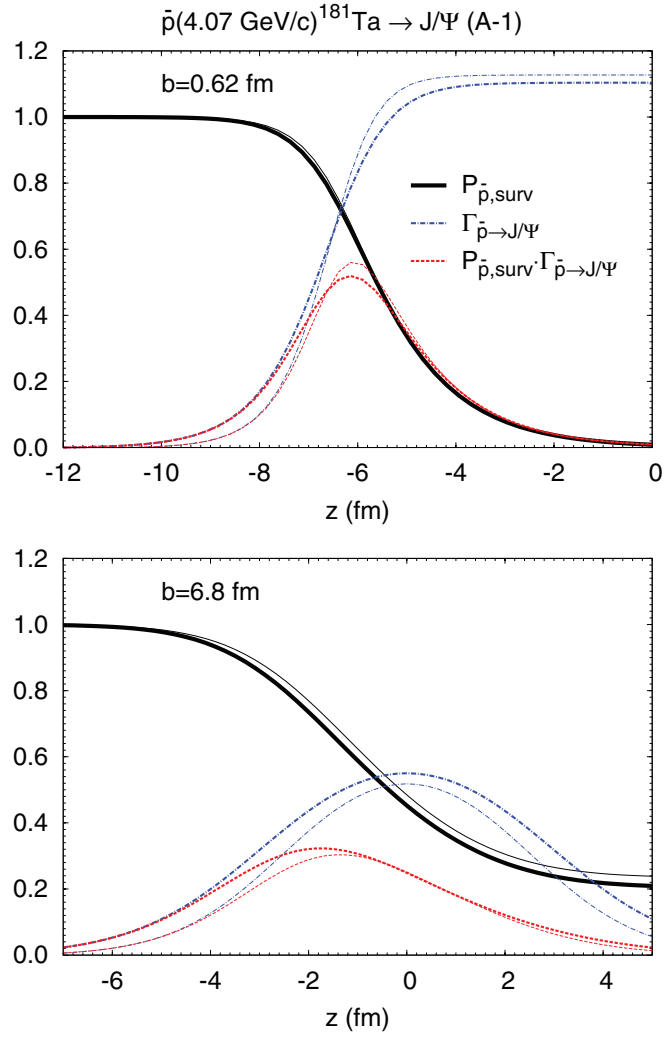

FIG. 1. (Color online) Dependence of the antiproton survival probability [Eq. (6), solid lines], of the J/Ψ production width [Eq. (19), dash-dotted lines], and of their product (dashed lines) on the longitudinal coordinate z for the central ($b = 0.62$ fm, upper panel) and peripheral ($b = 6.8$ fm, lower panel) collisions $\bar{p} + {}^{181}$Ta at $p_{\mathrm{lab}} = 4.07$ GeV/c. The width is given in units of 10^{-8} c/fm. The thick lines are obtained with the charge density diffuseness parameter $a_{\mathrm{ch}} = 0.64$ fm, while the thin lines with $a_{\mathrm{ch}} = 0.52$ fm. The center of the nucleus is at $b = 0$, $z = 0$. The antiproton propagates in the positive z direction.

width $\Gamma_{\bar{p}\to J/\Psi}$ is relatively small. Therefore, $\bar{p}$ absorption strongly (∼5 times) reduces the J/Ψ production governed by the product $P_{\bar{p},\mathrm{surv}}\Gamma_{\bar{p}\to J/\Psi}$. Moreover, the surface absorption of $\bar{p}$ leads to the significant sensitivity of J/Ψ production to the diffuseness of the proton density distribution, in particular for peripheral collisions (cf. thick and thin lines in the lower panel of Fig. 1). This sensitivity is more clearly demonstrated in Fig. 2, where the impact parameter dependence of the J/Ψ production probability (neglecting J/Ψ absorption)

$$P_{J/\Psi}(b) = v_{\bar{p}}^{-1}\int_{-\infty}^{\infty} dz P_{\bar{p},\mathrm{surv}}(z, b)\Gamma_{\bar{p}\to J/\Psi}(z, b) \tag{24}$$

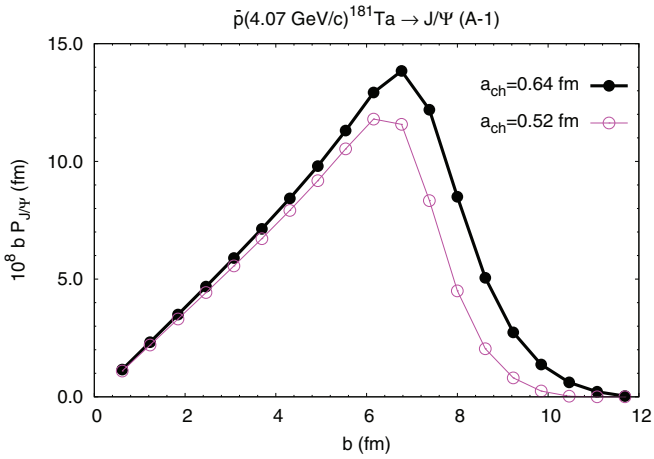

FIG. 2. (Color online) J/Ψ production probability [Eq. (24)] multiplied by impact parameter b as a function of b for $\bar{p} + {}^{181}\mathrm{Ta}$ collisions at $p_{\mathrm{lab}} = 4.07\,\mathrm{GeV}/c$. The lines with solid (open) circles are calculated with the charge density diffuseness parameter $a_{\mathrm{ch}} = 0.64$ (0.52) fm. J/Ψ absorption is turned off.

is shown for the two slightly different values of the charge density diffuseness parameter. The same effect shows up also in the mass dependence of the J/Ψ transparency ratio (upper panel of Fig. 4 below). Let us now discuss the impact-parameter integrated cross sections.

All cross sections have been calculated assuming the minimum bias triggering condition for the $\bar{p}$-nucleus collisions. Numerically, this has being done by setting the upper limit for the impact parameter integration in Eq. (2) equal to a large value, $R_n + 10a_n$ for all nuclei except ${}^{9}\mathrm{Be}$ and 8 fm for ${}^{9}\mathrm{Be}$.

Figure 3 shows the beam momentum dependence of the J/Ψ production cross section for several target nuclei. Apart from the result without J/Ψ absorption, we present two calculations with different $J/\Psi N$ dissociation cross sections. The choice $\sigma_{J/\Psi N} \simeq 3.5$ mb is motivated by the early experiment on J/Ψ photoproduction at $E_\gamma = 20\,\mathrm{GeV}$ at SLAC [10], while the value $\sigma_{J/\Psi N} \simeq 6$ mb is obtained in Ref. [2] from the global Glauber fit of the J/Ψ transparency ratios in high-energy γ-, p-, $\bar{p}$-, and π-induced reactions. The large $J/\Psi N$ inelastic cross section in the range 6–8 mb is reported in recent calculations employing effective Lagrangians of the local hidden gauge theory [22]. Since the J/Ψ formation length $l_{J/\Psi} \simeq 0.4$ fm at $p_{\mathrm{lab}} = 4\,\mathrm{GeV}/c$, the results are practically insensitive to the formation length effects, and we show only calculations with $l_{J/\Psi} = 0$ in Eq. (11). On the other hand, the final J/Ψ yield reveals a clear sensitivity to the $J/\Psi N$ dissociation cross section which becomes more pronounced for heavier targets.

In Fig. 4 we show the transparency ratio,

$$\tilde{S}_A = \frac{\sigma_{\bar{p}A\to R(A-1)^*}}{\sigma_{\bar{p}\,{}^{27}\mathrm{Al}\to R\,{}^{26}\mathrm{Mg}^*}} \left(\frac{27}{A}\right)^{2/3}, \tag{25}$$

calculated with the J/Ψ production cross sections at their peak values (see Fig. 3) and rescaled by $A^{-2/3}$. This rescaling factor corresponds to the surface-dominated $\bar{p}$ absorption at moderate beam momenta. The nucleus ${}^{27}\mathrm{Al}$ is chosen for normalization, since this is the lightest one in our set of selected

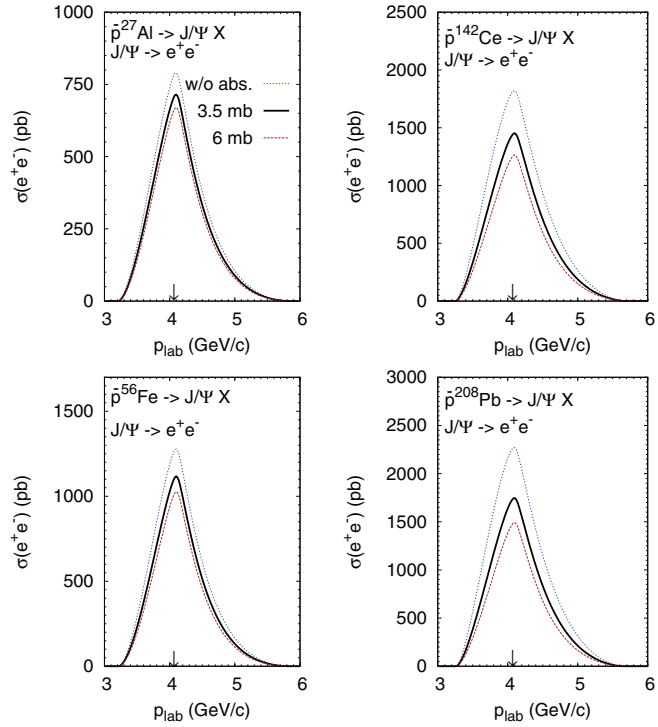

FIG. 3. (Color online) The J/Ψ production cross section in $\bar{p}$ collisions with ${}^{27}\mathrm{Al}$, ${}^{56}\mathrm{Fe}$, ${}^{142}\mathrm{Ce}$, and ${}^{208}\mathrm{Pb}$ vs antiproton beam momentum calculated with $\sigma_{J/\Psi N} = 0$ (dotted line), $\sigma_{J/\Psi N} = 3.5$ mb (solid line), and $\sigma_{J/\Psi N} = 6$ mb (dashed line). Vertical arrows show the beam momentum 4.07 GeV/c of the on-shell J/Ψ production in vacuum.

nuclei which has the two-parameter Fermi density distributions of nucleons. Being defined in this way, the transparency ratio better represents the systematic mass dependence for heavy nuclei.

The transparency ratio R_A reveals strong local variations as a function of the mass number when calculated with the empirical nucleon density parameters (upper panel of Fig. 4). This arises from the details of empirical density profiles. For example, the local maximum for the ${}^{181}\mathrm{Ta}$ nucleus appears due to the large diffuseness parameter of the charge distribution, $a_{\mathrm{ch}} = 0.64$ fm [20]. These local variations, as expected, disappear if we enforce the density profiles to be determined by the uniform parameters (lower panel of Fig. 4).

Another peculiar feature observed in Fig. 4 (upper panel) is a strong drop of the transparency ratio along the isotope chain ${}^{112-124}\mathrm{Sn}$. If we turn off absorption of both $\bar{p}$ and J/Ψ, then the cross section for J/Ψ production at the on-shell peak varies along this isotope chain by about 5% only, because the proton density distribution is similar for the different isotopes. Therefore, this drop is mostly caused by $\bar{p}$ absorption and J/Ψ dissociation on the neutron excess in heavier isotopes.

The sensitivity of the transparency ratio R_A to the input $J/\Psi N$ dissociation cross section is clearly visible in Fig. 4. The only possible strong interaction channels of the J/Ψ dissociation on a nucleon below $D\bar{D}$ production threshold ($p_{\mathrm{thr}} = 5.18\,\mathrm{GeV}/c$) are $J/\Psi N \to \Lambda_c \bar{D} +$ up to three pions. Hence, the J/Ψ dissociation cross section at the beam

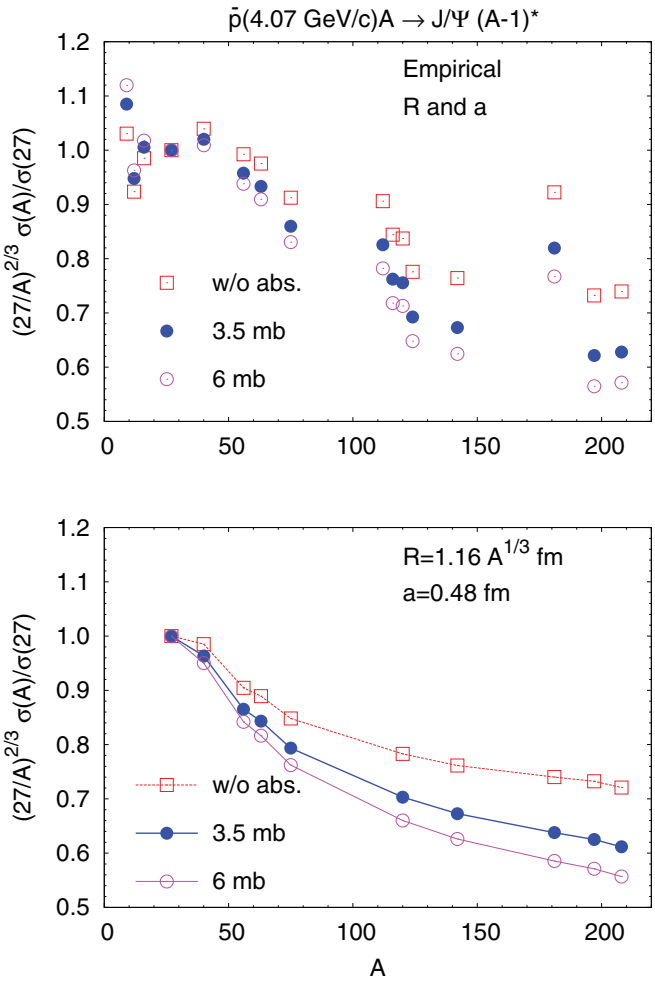

FIG. 4. (Color online) The transparency ratio of J/Ψ production in antiproton-induced reactions (25) for the nuclei ^{9}Be, ^{12}C, ^{16}O, ^{27}Al, ^{40}Ca, ^{56}Fe, ^{63}Cu, ^{75}As, ^{112,116,120,124}Sn, ^{142}Ce, ^{181}Ta, ^{197}Au, and ^{208}Pb plotted versus the mass number of the target nucleus. The ratio is normalized on 1 for ^{27}Al. Open squares and solid and open circles represent calculations with $\sigma_{J/\Psi N} = 0$, 3.5, and 6 mb, respectively. Upper panel: Results with density parameters R_q, a_q ($q = n, p$) determined for each nucleus separately as described at the beginning of Sec. III. Lower panel: Results for heavy nuclei excluding ^{112,116,124}Sn with $R_n = R_p = 1.16A^{1/3}$ fm and $a_n = a_p = 0.48$ fm.

momentum of $\simeq$4 GeV/c is equal to the inclusive $\Lambda_c\bar{D}$ production cross section on the nucleon. Moreover (see also Ref. [7]), both Λ_c and $\bar{D}$ cannot be absorbed in a nucleus for $p_{\rm lab} \simeq 4$ GeV/c but can only change momenta by rescattering on nucleons. For $\bar{D}$, the absorption is actually forbidden for any momentum by charm conservation in strong interactions. For Λ_c, the threshold momentum in the nucleon rest frame for the $\Lambda_c N \to NND$ is 3.55 GeV/c, while the maximum Λ_c momentum in $J/\Psi N \to \Lambda_c\bar{D}$ is 3.34 GeV/c. The direct channels $\bar{p}p \to D\bar{D}$ ($p_{\rm thr} = 6.45$ GeV/c) and $\bar{p}p \to \Lambda_c\bar{\Lambda}_c$ ($p_{\rm thr} = 10.16$ GeV/c) are not reachable at the J/Ψ production threshold. Therefore, the cross section of the $\Lambda_c\bar{D}$ pair production in $\bar{p}A$ collisions at $p_{\rm lab} \simeq 4$ GeV/c can be simply

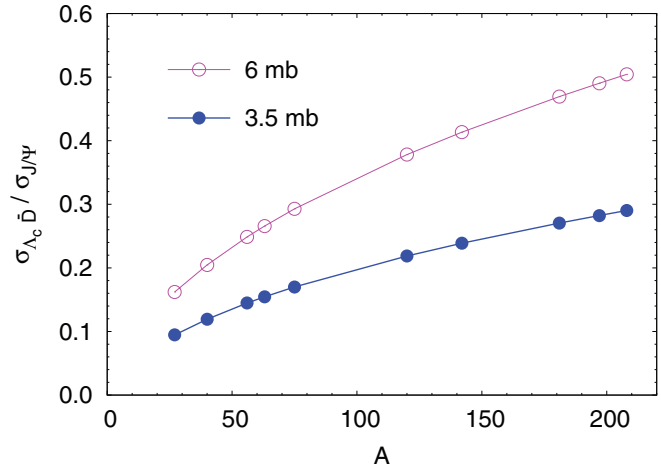

FIG. 5. (Color online) The ratio of the $\Lambda_c\bar{D}$ production cross section to the J/Ψ production cross section at $p_{\rm lab} = 4.07$ GeV/c for $\sigma_{J/\Psi N} = 3.5$ mb (full blue circles) and for $\sigma_{J/\Psi N} = 6$ mb (open purple circles). Heavy nuclei excluding ^{112,116,124}Sn are shown using $R_n = R_p = 1.16A^{1/3}$ fm and $a_n = a_p = 0.48$ fm.

calculated as

$$\sigma_{\Lambda_c\bar{D}} = \sigma^{\rm w/o\ J/\Psi abs.}_{\bar{p}A\to J/\Psi(A-1)^*} - \sigma_{\bar{p}A\to J/\Psi(A-1)^*}, \qquad (26)$$

where $\sigma_{\bar{p}A\to J/\Psi(A-1)^*}$ is given by Eq. (2) and $\sigma^{\rm w/o\ J/\Psi abs.}_{\bar{p}A\to J/\Psi(A-1)^*}$ by the same Eq. (2) but with $P_{J/\Psi,{\rm surv}} = 1$. In Fig. 5 we show the ratio $\sigma_{\Lambda_c\bar{D}}/\sigma_{\bar{p}A\to J/\Psi(A-1)^*}$ at the on-shell peak of the J/Ψ production vs target mass number. One sees the strong sensitivity of this ratio to the assumed value of the $J/\Psi N$ dissociation cross section.

We recall that the formation time effects are almost negligible and do not create an additional ambiguity for the J/Ψ production in low-energetic antiproton-nucleus reactions. In contrast, formation time effects are very important for the γ-induced J/Ψ production on nuclei. The transparency ratio in γ-induced reactions is defined according to Eq. (1), which in the simplest approximation is expressed as (cf. Ref. [2])

$$S_A = \frac{\sigma_{\gamma A\to J/\Psi X}}{A\sigma_{\gamma p\to J/\Psi X}} = \frac{2\pi}{A}\int_0^\infty db\, b \int_{-\infty}^\infty dz\rho(z,b)P_{J/\Psi,{\rm surv}}(z,b). \qquad (27)$$

This expression, however, is valid only at low photon energies, i.e., when the coherence length $l_c = 2E_\gamma/m^2_{J/\Psi}$ is much less than the nuclear radius. For $E_\gamma = 20$ and 120 GeV, where the J/Ψ production in photon-induced reactions is measured [10,11], the coherence length is already quite large, $l_c = 0.8$ and 4.8 fm, respectively. The deviations from the classical probabilistic formula (27) appear in the Glauber model due to the coherent addition of the production amplitudes on the two nucleons separated by the distance less than l_c [23,24]. In Refs. [23,24], the formulas have been derived which generalize Eq. (27) for arbitrary values of l_c (cf. Eqs. (4.2a) and (4.2b) in Ref. [23] and Eq. (13) in Ref. [24]). Similar expressions are also given in Refs. [25,26]. Although these expressions somewhat differ from each other (mainly because of the different assumptions on the vector meson-nucleon elastic

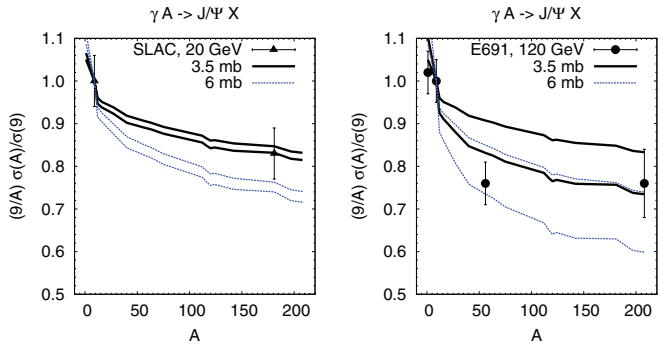

FIG. 6. (Color online) Transparency ratio S_A for the J/Ψ production in γ-induced reactions on nuclei vs target mass number. Left panel: $E_\gamma = 20$ GeV. Right panel: $E_\gamma = 120$ GeV. The results with $\sigma_{J/\Psi N} = 3.5$ mb and $\sigma_{J/\Psi N} = 6$ mb are shown by the solid and dashed lines, respectively. The lower and upper lines correspond to the calculations with formation length $l_{J/\Psi} = 0$ and $l_{J/\Psi} = 2(12)$ fm for $E_\gamma = 20(120)$ GeV. Experimental data points from SLAC at $E_\gamma = 20$ GeV (^{9}Be and ^{181}Ta targets) [10] and from Fermilab at $E_\gamma = 120$ GeV (p, ^{9}Be, ^{56}Fe, and ^{208}Pb targets) [11] represent the incoherent J/Ψ photoproduction cross section per nucleon normalized on 1 for ^{9}Be.

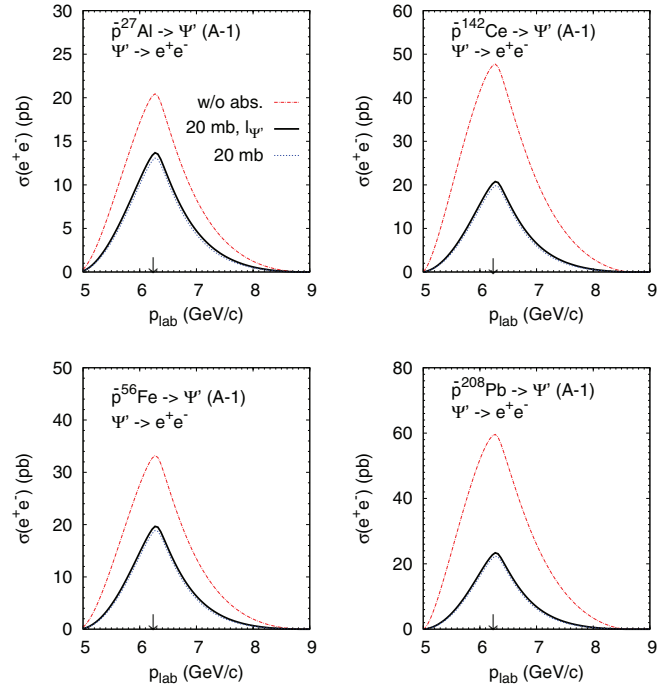

FIG. 7. (Color online) $\Psi'(2S)$ production cross section for $\bar{p}$ collisions with ^{27}Al, ^{56}Fe, ^{142}Ce, and ^{208}Pb vs antiproton beam momentum calculated with $\sigma_{\Psi' N} = 0$ (dash-dotted line) and $\sigma_{\Psi' N} = 20$ mb [4] with formation length $l_{\Psi'}$ defined according to Eq. (13) (solid line) and with $l_{\Psi'} = 0$ (dotted line). Vertical arrows show the antiproton beam momentum of the on-shell $\Psi'(2S)$ production in vacuum, $p_{\rm lab} = 6.23$ GeV.

cross section), they all give the same limits of $l_c \to 0$ and $l_c \to \infty$. In the former case one gets Eq. (27), while in the latter case one has to replace $P_{J/\Psi,\rm surv}(z, b) \to P_{J/\Psi,\rm surv}(-\infty, b)$ in (27). We will, thus, interpolate between these two limits by simply replacing $P_{J/\Psi,\rm surv}(z, b) \to P_{J/\Psi,\rm surv}(z - l_c, b)$ in Eq. (27). This should be a quite rough approximation, but it serves at least our purposes of the exploratory studies of the photoproduction.

Figure 6 shows the mass dependence of the transparency ratio S_A corrected for the coherence length effects. We present results for the two previous values of the $J/\Psi N$ dissociation cross section, $\sigma_{J/\Psi N} = 3.5$ and 6 mb. However, the charmonium formation length $l_{J/\Psi} = 2$ (12) fm at $p_{J/\Psi} = 20$ (120) GeV/c is comparable with the nuclear size. Thus, the effective cross section $\sigma^{\rm eff}_{J/\Psi N}$ of Eq. (11) is now substantially reduced with respect to $\sigma_{J/\Psi N}$ for the longitudinal coordinate within the nuclear target bulk region. The uncertainty in the determination of the charmonium formation length has an immediate feedback on the extraction of the genuine charmonium-nucleon dissociation cross section. As demonstrated in Fig. 6, for $E_\gamma = 20$ GeV, it is still possible to clearly see the differences among transparency ratios calculated with different values of $\sigma_{J/\Psi N}$. However, for $E_\gamma = 120$ GeV, the large formation length washes out the sensitivity of S_A to $\sigma_{J/\Psi N}$. Moreover, the experimental errors do not allow us to set tight constraints on $\sigma_{J/\Psi N}$.

Figures 7 and 8 present the beam momentum and mass number dependence of $\Psi'(2S)$ production in $\bar{p}$-induced reactions. Both dependencies are quite similar to those for J/Ψ production (cf. Figs. 3 and 4). The local variations of the transparency ratio (Fig. 8 upper panel) due to the empirical density profiles are again visible. The smooth behavior of the transparency ratio as a function of the mass number is recovered if we substitute the empirical density parameters by the uniform ones (Fig. 8 lower panel).

To provide some hints on the possible charmonium absorption effects, we show in Figs. 7 and 8 the calculations with $\sigma_{\Psi' N} = 20$ mb as theoretically estimated in Ref. [4]. This reduces the Ψ' yield by about a factor of 2–3 with respect to the calculation without Ψ' absorption. It is interesting to note that with such a strong absorption, the Ψ' production becomes almost independent of the target mass number.

Since the beam momentum is now larger than that for J/Ψ production, the formation length effects become visible (cf. solid and dotted lines in Fig. 7). However, they are still weak as compared to the uncertainty caused by the largely unknown $\Psi' N$ cross section.

Finally, we address the multistep processes which are not included in the Glauber model. For this purpose we have performed the GiBUU model [12] calculations of the $\bar{p}$ + ^{27}Al and $\bar{p}$ + ^{208}Pb reactions. The GiBUU model takes into account the annihilation as well as the elastic and inelastic rescattering of the incoming antiproton with empirical cross sections. The nuclear density profiles are chosen to be identical in both Glauber and GiBUU calculations. The antiproton-nucleon total and elastic cross sections (9) and (10) coincide in the both models as well. A comparison of the GiBUU and Glauber calculations is presented in Fig. 9. For simplicity, the nucleus was modeled in the local Fermi gas approximation in GiBUU. Therefore, for comparison purposes we have also performed the Glauber model calculations by doing the same assumption (solid lines in Fig. 9). This has been

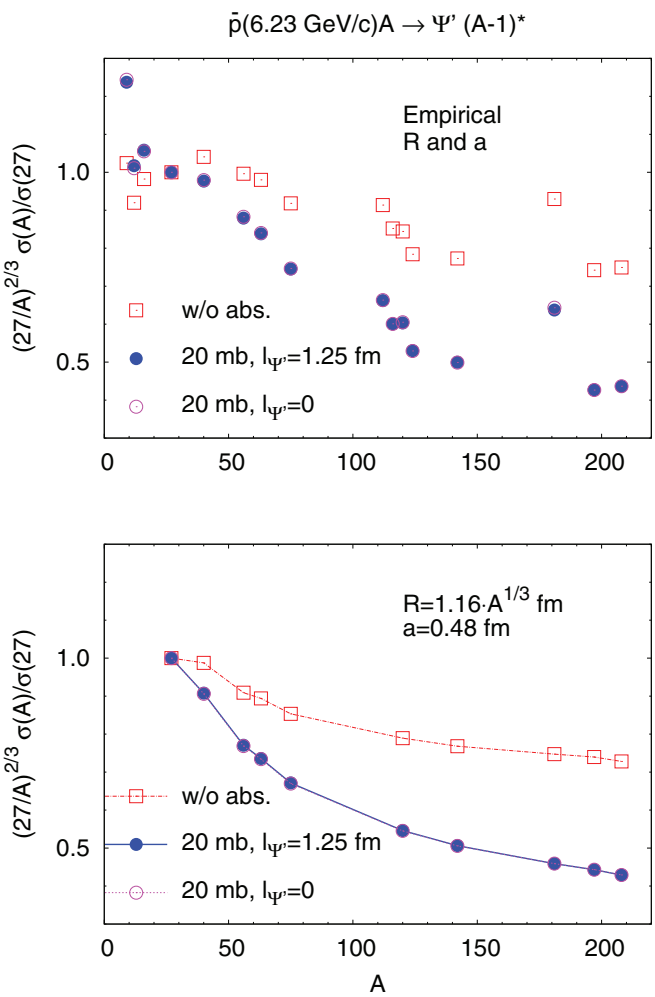

FIG. 8. (Color online) The transparency ratio of Ψ' production in antiproton-induced reactions (25) as a function of the target mass number. Open squares show the calculation without Ψ' absorption. Full and open circles represent the results with $\sigma_{\Psi' N} = 20$ mb [4] with Ψ' formation length $l_{\psi'}$ given by Eq. (13) at $p_{\rm lab} = 6.23$ GeV/c and with $l_{\psi'} = 0$, respectively. Upper panel: Calculations with empirical density parameters R_q, a_q $(q = n, p)$ (see the beginning of Sec. III). Lower panel: Calculations for heavy nuclei excluding ^{112,116,124}Sn with uniform density parameters $R_n = R_p = 1.16A^{1/3}$ fm and $a_n = a_p = 0.48$ fm.

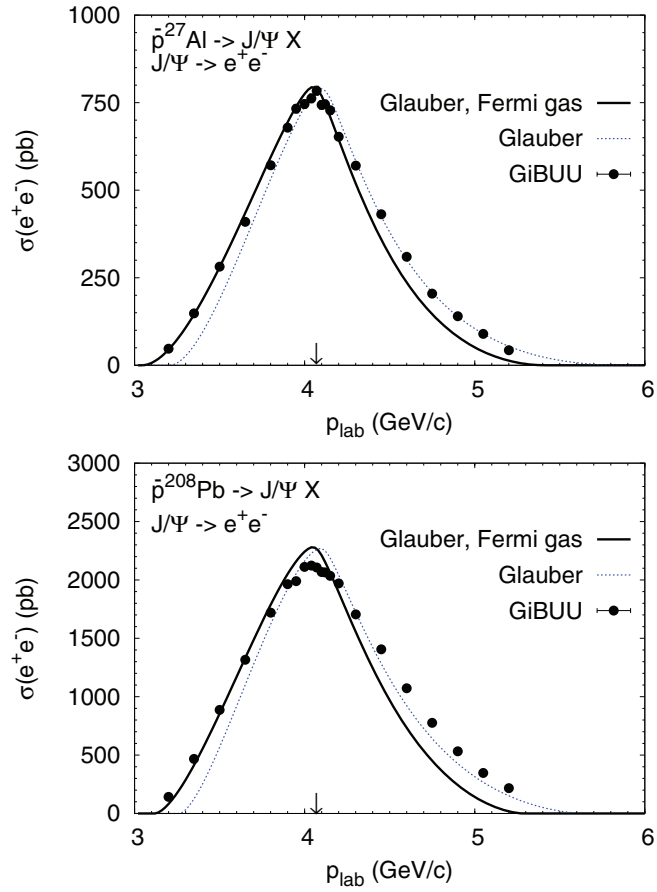

FIG. 9. (Color online) Comparison of the Glauber and GiBUU model calculations for the J/Ψ production cross section in $\bar{p}$ collisions with ^{27}Al and ^{208}Pb vs beam momentum. Dashed lines correspond to our standard Glauber model calculations with the fixed proton energy $E_p = m - B$ as described in Sec. II. Solid lines are obtained within the Glauber model assuming the local Fermi gas for the nuclear ground state, as in GiBUU. The J/Ψ absorption cross section is set to zero.

achieved by replacing Eq. (18) for the charmonium production width by the following formula:

$$\Gamma^{\rm FG}_{\bar{p}\to R} = \frac{3m_R^2\Gamma_{R\to\bar{p}p}}{4p_{\rm lab}E_{\bar{p}}q_R}\left[\sqrt{\min(p_2, p_{F,p})^2 + m^2} - \sqrt{\min(p_1, p_{F,p})^2 + m^2}\right], \quad (28)$$

where $p_{1,2} = |p_{\rm lab}(m_R^2 - 2m^2) \mp 2E_{\bar{p}}m_R q_R|/2m^2$. The Glauber calculation is quite close to the GiBUU results at the peak. However, at higher beam momenta the Glauber model (with the local Fermi gas assumption) underpredicts GiBUU somewhat. The reason is that the fast antiproton has a chance to be decelerated by elastic or inelastic collisions with nucleons and get momentum closer to the peak momentum, where the cross section of J/Ψ production is larger (see also discussion in Ref. [6]). This mechanism is taken into account in GiBUU while it is neglected in the Glauber model.

IV. CONCLUSIONS

We have performed the Glauber model calculations of $J/\Psi(1S)$ and $\Psi'(2S)$ charmonium production in $\bar{p}$-nucleus collisions at $p_{\rm lab} = 3$–10 GeV/c. For both charmonia, we have focused on the beam momentum range near the corresponding on-shell production peaks. Thus, only the $\bar{p}p \to R$ channel was taken into account. The main nuclear effect is the broadening and reduction of the narrow charmonium production peak due to the nuclear Fermi motion.

The J/Ψ production cross section in $\bar{p}A$ collisions strongly depends on the input $J/\Psi N$ dissociation cross section. This dependence is not blurred by the charmonium formation

length, in contrast to J/Ψ production in γ-induced reactions at high energies.

The surface-dominated antiproton absorption leads to relatively large local variations of the J/Ψ transparency ratios as a function of the target mass number. This is due to the delicate interplay between the neutron and proton density profiles: The former governs the absorption range of the antiproton, while the latter defines the space region, where the J/Ψ is produced. We conclude that the quantitative determination of the $J/\Psi N$ dissociation cross section from experimental data on J/Ψ production in $\bar{p}A$ reactions relies on the detailed and realistic description of the neutron and proton density distributions.

We note at this point that the spreading of the proton momentum distribution due to the short-range correlations has not been taken into account in the present calculations. Although these effects are very important at extreme kinematics regions, they will not sensitively modify our results near the on-shell peaks of charmonium production. The reason is that in this case the momentum integration in Eq. (3) is not restricted from the low-momentum side and, hence, is only weakly sensitive to the high-momentum tail. Another reason is that the short-range correlations become weaker at the nuclear surface, where the antiproton is predominantly absorbed. Overall, the short-range correlations may create the additional uncertainty of $\sim$10% in the cross sections of the charmonium production close to the peak value. The same is true for the multistep effects due to the rescattering of the incoming antiproton in heavy target nuclei (Fig. 9).

It is expected from QCD that the $\Psi' N$ cross section is a factor of 2–4 larger than the $J/\Psi N$ cross section due to the larger size of the Ψ' as compared to the J/Ψ and it may reach up to 20 mb [4,27]. Such a strong absorption will be certainly testable with the new PANDA detector at FAIR beginning in 2018. Having all the above uncertainties of our calculations in mind, we conclude that the measurements of the J/Ψ transparency ratio with a precision of at least $\sim$20% would allow determination of the J/Ψ-nucleon dissociation cross section with accuracy of about 3 mb.

A significant $J/\Psi N$ cross section implies the corresponding enhancement of $\Lambda_c \bar{D}$ production, since near the J/Ψ production threshold $J/\Psi N \to \Lambda_c \bar{D}$ is the only possible inelastic channel of the $J/\Psi N$ interaction. On the other hand, there are several models which give widely spread predictions for the $J/\Psi N \to \Lambda_c \bar{D}$ cross sections [22,28–30]. Thus, PANDA offers an interesting possibility to test these predictions by measuring the ratio of the $\Lambda_c \bar{D}$-to-J/Ψ-production cross sections (cf. Fig. 5).

ACKNOWLEDGMENTS

A.L. acknowledges useful discussions with H. Lenske and U. Mosel and the hospitality and financial support of Giessen University, where this work was initiated. M.S. wants to thank the Helmholtz Institute in Mainz for support during the initial stage of work on this project. This work was supported by HIC for FAIR within the framework of the LOEWE program (Germany) and by Grant No. NSH-215.2012.2 (Russia).

[1] T. Matsui and H. Satz, Phys. Lett. B **178**, 416 (1986).
[2] C. Gerschel and J. Hüfner, Z. Phys. C **56**, 171 (1992).
[3] D. Kharzeev, C. Lourenco, M. Nardi, and H. Satz, Z. Phys. C **74**, 307 (1997).
[4] L. Gerland, L. Frankfurt, M. Strikman, H. Stöcker, and W. Greiner, Phys. Rev. Lett. **81**, 762 (1998).
[5] S. J. Brodsky and A. H. Mueller, Phys. Lett. B **206**, 685 (1988).
[6] G. R. Farrar, L. L. Frankfurt, M. I. Strikman, and H. Liu, Nucl. Phys. B **345**, 125 (1990).
[7] L. Gerland, L. Frankfurt, and M. Strikman, Phys. Lett. B **619**, 95 (2005).
[8] K. K. Seth, in *Proceedings of the 29th International Workshop on Gross Properties of Nuclei and Nuclear Excitations, 14–20 Jan. 2001, Hirschegg, Austria*, edited by H. Feldmeier, J. Knoll, W. Norenberg, and J. Wambach (GSI, Darmstadt, 2001), p. 183.
[9] W. Erni *et al.* (The PANDA Collaboration), M. F. M. Lutz, B. Pire, O. Scholten, and R. Timmermans, arXiv:0903.3905 (2009).
[10] R. L. Anderson *et al.*, Phys. Rev. Lett. **38**, 263 (1977).
[11] M. D. Sokoloff *et al.*, Phys. Rev. Lett. **57**, 3003 (1986).
[12] O. Buss, T. Gaitanos, K. Gallmeister, H. van Hees, M. Kaskulov *et al.*, Phys. Rept. **512**, 1 (2012).
[13] J. Arrington, D. Higinbotham, G. Rosner, and M. Sargsian, Prog. Part. Nucl. Phys. **67**, 898 (2012).
[14] L. Montanet *et al.* (ParticleDataGroup), Phys. Rev. D **50**, 1173 (1994).
[15] G. R. Farrar, H. Liu, L. L. Frankfurt, and M. I. Strikman, Phys. Rev. Lett. **61**, 686 (1988).
[16] G. Audi, A. Wapstra, and C. Thibault, Nucl. Phys. A **729**, 337 (2002).
[17] V. P. Koptev, E. M. Maev, M. M. Makarov, and A. V. Khanzadeev, Yad. Fiz. **31**, 1501 (1980) [Sov. J. Nucl. Phys. **31**, 779 (1980)].
[18] J. Nieves, E. Oset, and C. Garcia-Recio, Nucl. Phys. A **554**, 509 (1993).
[19] R. Schmidt, A. Trzcinska, T. Czosnyka, T. von Egidy, K. Gulda *et al.*, Phys. Rev. C **67**, 044308 (2003).
[20] C. De Jager, H. De Vries, and C. De Vries, At. Data Nucl. Data Tables **14**, 479 (1974).
[21] J. W. Negele and D. Vautherin, Phys. Rev. C **5**, 1472 (1972).
[22] R. Molina, C. W. Xiao, and E. Oset, Phys. Rev. C **86**, 014604 (2012).
[23] T. H. Bauer, R. D. Spital, D. R. Yennie, and F. M. Pipkin, Rev. Mod. Phys. **50**, 261 (1978).
[24] J. Hüfner, B. Kopeliovich, and J. Nemchik, Phys. Lett. B **383**, 362 (1996).
[25] J. Hüfner, B. Kopeliovich, and A. B. Zamolodchikov, Z. Phys. A **357**, 113 (1997).
[26] Yu. P. Ivanov, B. Z. Kopeliovich, A. V. Tarasov, and J. Hüfner, Phys. Rev. C **66**, 024903 (2002).
[27] J. Hüfner and B. Z. Kopeliovich, Phys. Lett. B **426**, 154 (1998).
[28] A. Sibirtsev, K. Tsushima, and A. W. Thomas, Phys. Rev. C **63**, 044906 (2001).
[29] Y. Oh, W. Liu, and C. M. Ko, Phys. Rev. C **75**, 064903 (2007).
[30] J. P. Hilbert, N. Black, T. Barnes, and E. S. Swanson, Phys. Rev. C **75**, 064907 (2007).